We are IntechOpen, the world's leading publisher of Open Access books Built by scientists, for scientists

6,900
Open access books available

186,000
International authors and editors

200M
Downloads

154
Countries delivered to

Our authors are among the

TOP 1%
most cited scientists

12.2%
Contributors from top 500 universities

CLARIVATE ANALYTICS
BOOK CITATION INDEX
INDEXED

WEB OF SCIENCE™

Selection of our books indexed in the Book Citation Index
in Web of Science™ Core Collection (BKCI)

Interested in publishing with us?
Contact book.department@intechopen.com

Nonlinear Model-Based Control of a Parallel Robot Driven by Pneumatic Muscle Actuators

Harald Aschemann and Dominik Schindele
Chair of Mechatronics, University of Rostock
18059 Rostock,
Germany

1. Introduction

In this contribution, three nonlinear control strategies are presented for a two-degree-of-freedom parallel robot that is actuated by two pairs of pneumatic muscle actuators as depicted in Fig. 1. Pneumatic muscles are innovative tensile actuators consisting of a fibre-reinforced vulcanised rubber hose with appropriate connectors at both ends. The working principle is based on a rhombical fibre structure that leads to a muscle contraction in longitudinal direction when the pneumatic muscle is filled with compressed air. Pneumatic muscles are low cost actuators and offer several further advantages in comparison to classical pneumatic cylinders: significantly less weight, no stick-slip effects, insensitivity to dirty working environment, and a higher force-to-weight ratio. The achievable closed-loop performance using such actuators has already been investigated experimentally at a linear axis with a pair of antagonistically arranged pneumatic muscles (Aschemann & Hofer, 2004). Current research activities concentrate on the use of pneumatic muscles as actuators for parallel robots, which are known for providing high stiffness, and especially for the capability of performing fast and highly accurate motions of the end-effector. The planar parallel robot under consideration is characterised by a closed-chain kinematic structure formed by four moving links and the robot base, which offers two degrees of freedom, see Fig. 1. All joints are revolute joints, two of which - the cranks - are actuated by a pair of pneumatic muscles, respectively. The coordinated contractions of a pair of pneumatic muscles are transformed into a rotation of the according crank by means of a toothed belt and a pulley. The mass flow rate of compressed air is provided by a separate proportional valve for each pneumatic muscle.

The paper is structured as follows: first, a mathematical model of the mechatronic system is derived, which results in a symbolic nonlinear state space description. Second, a cascaded control structure is proposed: the control design for the inner control loops involves a decentralised pressure control for each pneumatic muscle with high bandwidth, whereas the design of the outer control loop deals with decoupling control of the two crank angles and the two mean pressures of both pairs of pneumatic muscles. For the inner control loops nonlinear pressure controls are designed taking advantage of differential flatness. For the outer control loop three alternative approaches have been investigated: flatness-based control, backstepping, and sliding-mode control. Third, to account for nonlinear friction as

well as model uncertainties, a nonlinear reduced order disturbance observer is used in a disturbance compensation scheme. Simulation results of the closed-loop system show excellent tracking performance and high steady-state accuracy.
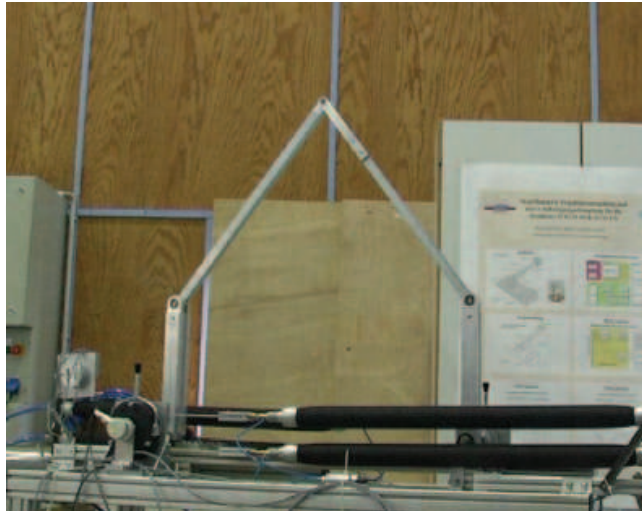

Fig. 1. Test rig.

2. System modelling

The modelling of the pneumatically driven parallel robot involves the mechanical subsystem and the pneumatic subsystem, which are coupled by the torques resulting from the tension forces of a pair of pneumatic muscles, respectively.

2.1 Multibody model of the parallel robot

The control-oriented multibody model of the parallel robot part consists of three rigid bodies (Fig. 2): the two cranks as actuated links with identical properties (mass m_A, reduced mass moment of inertia w.r.t. the actuated axis J_A, centre of gravity distance s_A to the centre of gravity, length of the link l_A, pulley radius r) and the end-effector E (mass m_E), which is modelled as lumped mass.
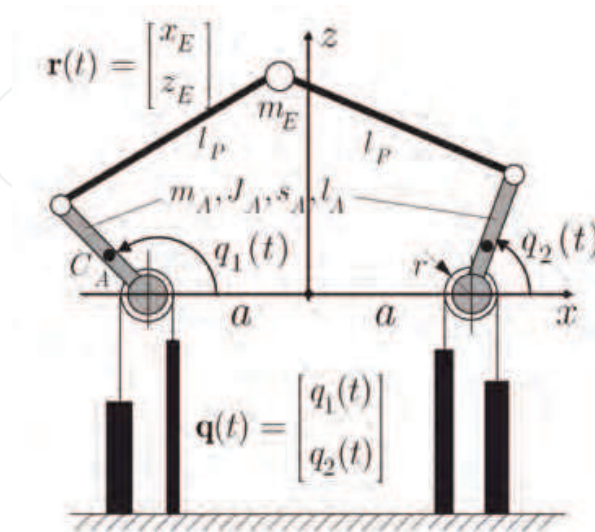

Fig. 2. Multibody model of the parallel robot.

The inertia properties of the remaining two links with length l_P, which are designed as light-weight construction, shall be neglected in comparison to the other links. The inertial xz-coordinate system is chosen in the middle of the straight line that connects both base joints. The motion of the parallel robot is completely described by two generalised coordinates $q_1(t)$ and $q_2(t)$ that denote the two crank angles, which are combined in the vector $\mathbf{q} = [q_1, q_2]^T$. Analogously, the vector of the end-effector coordinates is defined as $\mathbf{r} = [x_E, z_E]^T$.
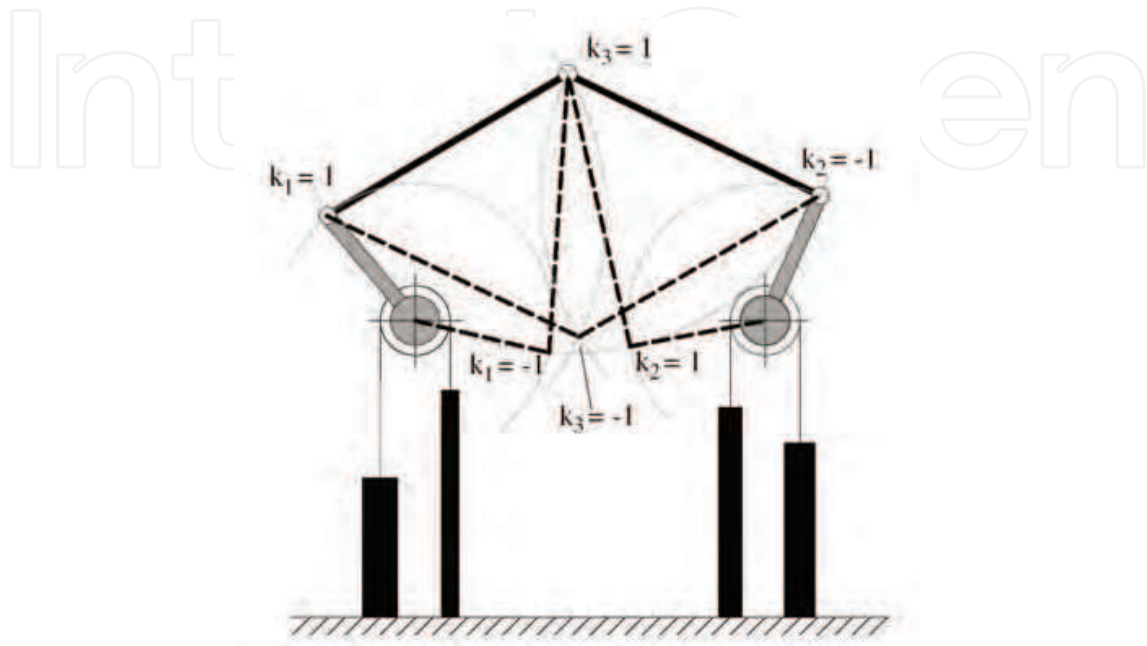

Fig. 3. Ambiguity of the robot kinematics.

The direct kinematics can be stated in symbolic form and describes the vector of end-effector coordinates $\mathbf{r}$ in terms of given crank angles $\mathbf{q}$, i.e.

$$\mathbf{r} = \mathbf{r}(\mathbf{q}, k_3). \tag{1}$$

Here, the configuration parameter k_3 is introduced to cope with two possible configurations, see Fig. 3. The relationship between the corresponding velocities is obtained by differentiation with respect to time

$$\dot{\mathbf{r}} = \mathbf{J}(\mathbf{q}, k_3)\,\dot{\mathbf{q}}, \quad \mathbf{J}(\mathbf{q}, k_3) = \frac{\partial \mathbf{r}(\mathbf{q}, k_3)}{\partial \mathbf{q}^T}, \tag{2}$$

where $\mathbf{J}(\mathbf{q}, k_3)$ denotes the corresponding Jacobian. Here, singularities in the Jacobian can be avoided by model-based trajectory planning. Analogously, the acceleration relationship is given by

$$\ddot{\mathbf{r}} = \mathbf{J}(\mathbf{q}, k_3)\ddot{\mathbf{q}} + \dot{\mathbf{J}}(\mathbf{q}, k_3)\,\dot{\mathbf{q}}. \tag{3}$$

For a given end-effector position $\mathbf{r}$ the corresponding crank angles follow from the inverse kinematics

$$\mathbf{q} = \mathbf{q}(\mathbf{r}, k_1, k_2), \tag{4}$$

which can be determined in symbolic form. The given ambiguity is taken into account by introducing two configuration parameters k_1 and k_2 as shown in Fig. 3. The relationships between the corresponding velocities as well as the accelerations follow from direct kinematics

$$
\begin{aligned}
\dot{\mathbf{q}} &= \mathbf{J}^{-1}(\mathbf{r}, k_3)\, \dot{\mathbf{r}}, \\
\ddot{\mathbf{q}} &= \mathbf{J}^{-1}(\mathbf{q}, k_3)\, [\ddot{\mathbf{r}} - \dot{\mathbf{J}}(\mathbf{q}, k_3)\, \dot{\mathbf{q}}].
\end{aligned}
\tag{5}
$$

Fig. 4. Free-body diagram of the parallel robot.

The equations of motion for the actuated links can be directly derived from the free-body diagram in Fig. 4 applying the principle of angular momentum

$$
\begin{aligned}
J_A \cdot \ddot{q}_1 &= \underbrace{r \cdot [F_{M1l} - F_{M1r}]}_{\tau_1} - m_A \cdot g \cdot s_A \cdot \cos q_1 + F_{1E} \cdot l_A \cdot \sin \beta_1 + \eta_1 \,, \\
J_A \cdot \ddot{q}_2 &= \underbrace{r \cdot [F_{M2l} - F_{M2r}]}_{\tau_2} - m_A \cdot g \cdot s_A \cdot \cos q_2 - F_{2E} \cdot l_A \cdot \sin \beta_2 + \eta_2 \,.
\end{aligned}
\tag{6}
$$

Here, the driving torque τ_i of drive i depends on the corresponding muscle forces, i.e. $\tau_i = r [F_{Mil} - F_{Mir}]$. At this, the indices of all variables describing a particular pneumatic muscle are chosen as follows: the first index $i = \{1, 2\}$ denotes the drive under consideration, described by the generalised coordinate $q_i(t)$, whereas the second index $j = \{l, r\}$ stands for the mounting position, i.e. for the left or the right pneumatic muscle. The disturbance torque η_i accounts for friction effects as well as remaining uncertainties in the muscle force characteristics (13) of drive i, respectively. The coupling forces F_{1E} and F_{2E} are obtained from Newton's second law applied to the end-effector

$$
\begin{bmatrix} m_E \cdot \ddot{x}_E \\ m_E \cdot (g + \ddot{z}_E) \end{bmatrix} = \begin{bmatrix} \cos \gamma_1 & -\cos \gamma_2 \\ \sin \gamma_1 & \sin \gamma_2 \end{bmatrix} \begin{bmatrix} F_{1E} \\ F_{2E} \end{bmatrix}.
\tag{7}
$$

The equations of motion in minimal form for the crank angles can be derived in two steps. First, the last equation has to be solved for the unknown forces

$$\begin{bmatrix} F_{1E} \\ F_{2E} \end{bmatrix} = \begin{bmatrix} \cos\gamma_1 & -\cos\gamma_2 \\ \sin\gamma_1 & \sin\gamma_2 \end{bmatrix}^{-1} \begin{bmatrix} m_E \cdot \ddot{x}_E \\ m_E \cdot (g + \ddot{z}_E) \end{bmatrix}, \tag{8}$$

which then can be eliminated in (6). Second, the substitution of the variables $\gamma_i = \gamma_i(\mathbf{q})$, $\beta_i = \beta_i(\mathbf{q})$, and (3) resulting from direct kinematics leads to the envisaged minimal form of the equations of motion

$$\mathbf{M(q)\ddot{q}} + \mathbf{k(q,\dot{q})} + \mathbf{G(q)} = \mathbf{Q(q)}, \tag{9}$$

with the mass matrix $\mathbf{M(q)}$, the vector of centrifugal and Coriolis terms $\mathbf{k(q,\dot{q})}$ and the vector of gravity torques $\mathbf{G(q)}$. The vector of generalised torques $\mathbf{Q(q)}$ contains the corresponding muscle forces times the radius r of the pulley

$$\mathbf{Q(q)} = r \cdot \begin{bmatrix} F_{M1l} - F_{M1r} \\ F_{M2l} - F_{M2r} \end{bmatrix}. \tag{10}$$

Note that this minimal form of the equations of motions is not compulsory. Instead the corresponding system of differential-algebraic equations can be utilised as well for the flatness-based control design.

2.2 Modelling of the pneumatic subsystem

The parallel robot is equipped with four pneumatic muscle actuators. The contraction lengths of the pneumatic muscles are related to the generalised coordinates, i.e. the crank angles q_i. The position of the crank angle, where the corresponding right pneumatic muscle is fully contracted, is denoted by q_{i0}. Consequently, by considering the transmission consisting of toothed belt and pulley, the following constraints hold for the contraction lengths of the muscles

$$\begin{aligned} \Delta\ell_{Mil}(q_i) &= r \cdot (q_i - q_{i0}), \\ \Delta\ell_{Mir}(q_i) &= \Delta\ell_{M,\max} - r \cdot (q_i - q_{i0}). \end{aligned} \tag{11}$$

Here, $\Delta\ell_{M,\max}$ is the maximum contraction given by 25% of the uncontracted length.

The volume characteristic of the pneumatic muscle (Fig. 5) can be approximated with high accuracy by the following nonlinear function of both contraction length and muscle pressure, where the coefficients in this polynomial approximation have been identified by measurements

$$V(\Delta\ell_{Mij}, p_{Mij}) = \sum_{m=0}^{3} \left(a_m \cdot \Delta\ell_{Mij}^m \right) \cdot \sum_{n=0}^{1} \left(b_n \cdot p_{Mij}^n \right). \tag{12}$$

The force characteristic $F_{Mij}(p_{Mij}, \Delta\ell_{Mij})$ of the pneumatic muscle shown in Fig. 6 describes the resulting static tension force for given internal pressure p_{Mij} as well as given contraction length $\Delta\ell_{Mij}$. This nonlinear force characteristic has been identified by static measurements and, then, approximated by the following polynomial description

$$F_{Mij} = \overline{F}_{Mij}(\Delta\ell_{Mij}) \cdot p_{Mij} - f_{Mij}(\Delta\ell_{Mij}) = \sum_{m=0}^{3} \left(c_m \cdot \Delta\ell_{Mij}^m \right) \cdot p_{Mi} - \sum_{n=0}^{4} \left(d_n \cdot \Delta\ell_{Mij}^n \right). \tag{13}$$
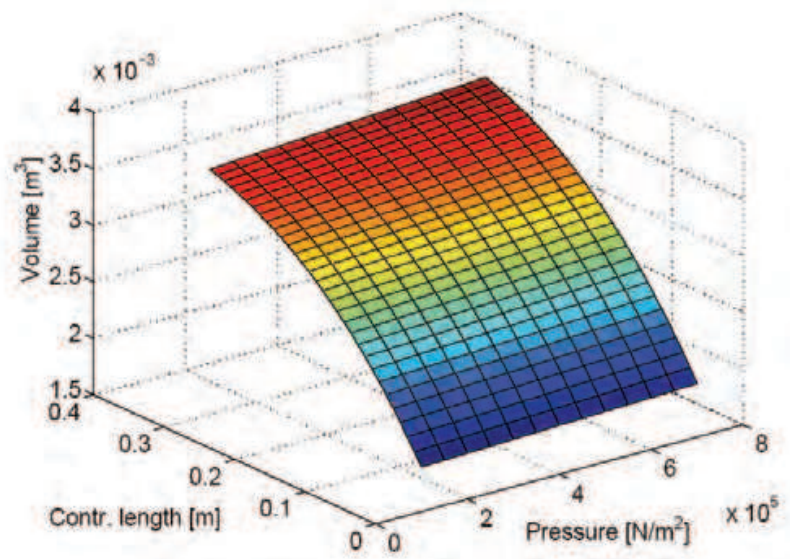
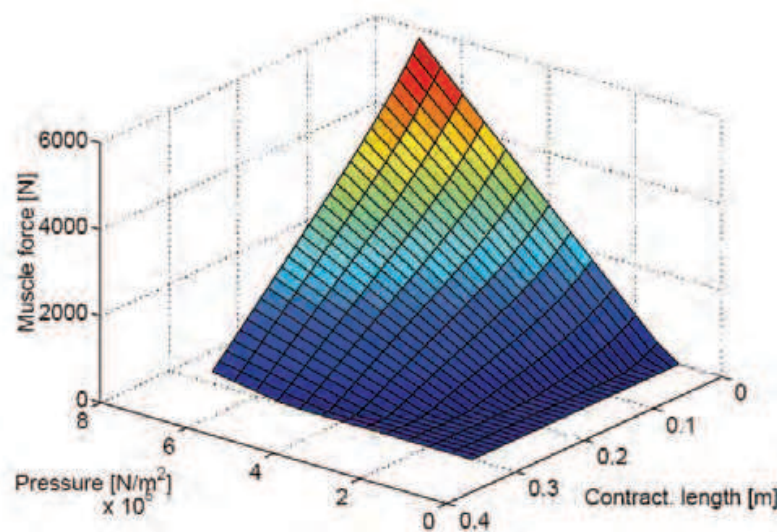Fig. 5. Volume characteristic of a pneumatic muscle.

Fig. 6. Force characteristic of a pneumatic muscle.

The dynamics of the internal muscle pressure follows directly from a mass flow balance in combination with the pressure-density relationship. As the maximum internal muscle pressure is limited by a maximum value of p_{max} = 7 bar, the ideal gas equation can be utilised as accurate description of the thermodynamic behaviour of the compressed air

$$p_{Mij} = R \cdot T_{Mij} \cdot \rho_{Mij} .$$ (14)

Here, the density ρ_{Mij} , the gas constant R of air, and the thermodynamic temperature T_{Mij} are introduced. For the thermodynamic process a polytropic change of state is assumed. Thus, the relationship between the time derivative of the pressure and the time derivative of the density results in

$$\dot{p}_{Mij} = n \cdot R \cdot T_{Mij} \cdot \dot{\rho}_{Mij} .$$ (15)

The mass flow balance for the pneumatic muscle is governed by

$$\dot{\rho}_{Mij} = \frac{1}{V_{Mij}\left(\Delta\ell_{Mij}, p_{Mij}\right)}\left[\dot{m}_{Mij} - \rho_{Mij} \cdot \dot{V}_{Mij}\left(\Delta\ell_{Mij}, p_{Mij}\right)\right]. \tag{16}$$

The resulting pressure dynamics is given by a nonlinear first order differential equation and shall not be neglected as in (Carbonell et. al., 2001)

$$\dot{p}_{Mij} = \frac{1}{V_{Mij} + n \cdot \dfrac{\partial V_{Mij}}{\partial p_{Mij}} \cdot p_{Mij}} \cdot \left[R \cdot T_{Mij} \cdot \dot{m}_{Mij} - \frac{\partial V_{Mij}}{\partial \Delta\ell_{Mij}} \cdot \frac{\partial \Delta\ell_{Mij}}{\partial q_i} \cdot p_{Mij} \cdot \dot{q}_i \right]. \tag{17}$$

The internal temperature T_{Mij} can be approximated with good accuracy by the constant temperature T_0 of the ambiance (Göttert, 2004). Thereby, temperature measurements can be avoided, and the implementational effort is significantly reduced.

3. Control design based on differential flatness

A nonlinear system in state space notation is denoted as differentially flat (Fliess et. al., 1995), if flat outputs

$$\mathbf{y} = \mathbf{y}(\mathbf{x}, \mathbf{u}, \dot{\mathbf{u}}, ..., \mathbf{u}^{(\alpha)}), \quad \dim(\mathbf{y}) = \dim(\mathbf{u}) \tag{18}$$

exist that allow for expressing all system states $\mathbf{x}$ and all system inputs $\mathbf{u}$ in the form

$$\begin{aligned} \mathbf{x} &= \mathbf{x}(\mathbf{y}, \dot{\mathbf{y}}, ..., \mathbf{y}^{(\beta)}), \\ \mathbf{u} &= \mathbf{u}(\mathbf{y}, \dot{\mathbf{y}}, ..., \mathbf{y}^{(\beta+1)}). \end{aligned} \tag{19}$$

As a result, offline trajectory planning considering state and input constraints become possible. Moreover, the stated parametrization of the complete system dynamics by the flat outputs can be exploited for pure feedforward control as well as combined feedforward and feedback control.

3.1 Flatness-based pressure control

The nonlinear state equation (17) for the internal muscle pressure p_{Mij} represents the basis for the decentralized pressure control. It can be re-formulated as

$$\dot{p}_{Mij} = -k_{pij}\left(\Delta\ell_{Mij}, \Delta\dot{\ell}_{Mij}, p_{Mij}\right) \cdot p_{Mij} + k_{uij}\left(\Delta\ell_{Mij}, p_{Mij}\right) \cdot \dot{m}_{Mij}. \tag{20}$$

With the internal muscle pressure as flat output candidate $y_{ijp} = p_{Mij}$, (20) can be solved for the mass flow $\dot{m}_{Mij}$ as control input u_{ijp} and leads to the inverse model for the pressure control

$$\dot{m}_{Mij} = \frac{1}{k_{uij}\left(\Delta\ell_{Mij}, p_{Mij}\right)} \cdot \left[v_{ij} + k_{pij}\left(\Delta\ell_{Mij}, \Delta\dot{\ell}_{Mij}, p_{Mij}\right) \cdot p_{Mij} \right], \tag{21}$$

Since the internal pressure p_{Mij} as state variable is identical to the flat output and $\dim(y_{ijp}) = \dim(u_{ijp}) = 1$ holds, the differential flatness property is proven. The contraction length $\Delta\ell_{Mij}$ as well as its time derivative can be considered as scheduling parameters in a gain-scheduled adaptation of k_{uij} and k_{pij}. With the internal pressure as flat output, its first time derivative is introduced as new control input

$$\dot{p}_{Mij} = v_{ij} \,. \tag{22}$$

Consequently, the state variable of the corresponding Brunovsky form has to be provided by means of measurements, i.e. $z_{ijp} = p_{Mij}$. Each pneumatic muscle is equipped with a pressure transducer mounted at the connection flange that connects the muscle with the toothed belt. For the contraction length and its time derivative either measured or desired values can be employed: in the given implementation, the scheduling parameter $\Delta\ell_{Mij}$ results from the measured crank angle q_i, which is obtained by an encoder providing high resolution. Furthermore, the second scheduling parameter, the contraction velocity, is derived from the crank angle q_i by means of real differentiation using a DT_1-System with the corresponding transfer function

$$G_{DT1}(s) = \frac{s}{T_1 \cdot s + 1} \,. \tag{23}$$

The error dynamics of each muscle pressure p_{Mij} can be asymptotically stabilised by the following control law which is evaluated with the measured pressure. Using this control law all nonlinearities are compensated for. An asymptotically stable error dynamics is obtained by pole placement

$$\left.\begin{aligned} \dot{p}_{Mij} &= v_{ij} \\ v_{ij} &= \dot{p}_{Mijd} + \alpha_{10}(p_{Mijd} - p_{Mij}) \end{aligned}\right\} \;\Rightarrow\; \dot{e}_{pij} + \alpha_{10} \cdot e_{pij} = 0 \,, \tag{24}$$

where the constant α_{10} is determined by pole placement. Here, the desired value for the time derivative of the internal muscle pressure can be obtained either by real differentiation of the corresponding control input u_{ij} in (33) or by model-based calculation using only desired values, i.e.

$$\dot{p}_{Mijd} = \dot{p}_{Mijd}(\mathbf{r}, \dot{\mathbf{r}}, \ddot{\mathbf{r}}, p_{Mid}, \dot{p}_{Mid}) \,. \tag{25}$$

The corresponding desired trajectories are obtained from a trajectory planning module that provides synchronous time optimal trajectories according to given kinematic and dynamic constraints (Aschemann & Hofer, 2005). It becomes obvious that a continuous time derivative $\dot{p}_{Mijd}$ requires a three times continuously differentiable desired end-effector trajectory $\mathbf{r}$.

The implementation of the underlying flatness-based pressure control structure for drive i is depicted in Fig. 7. In each input channel, the nonlinear valve characteristic (VC) is compensated by pre-multiplying with its approximated inverse valve characteristic (IVC). This inverse valve characteristic is implemented as look-up-table and depends both on the commanded mass flow and on the measured internal pressure.
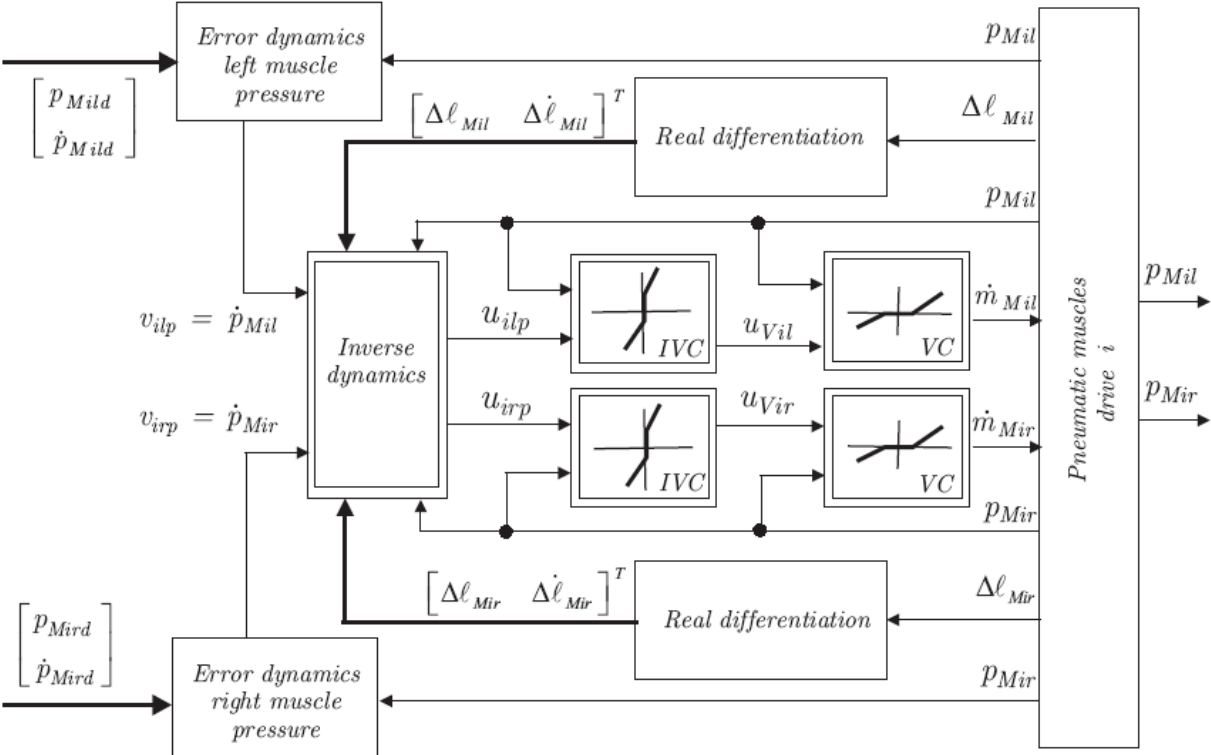
Fig. 7. Implementation of the underlying pressure control structure for drive i.

3.2 Inverse dynamics of the decoupling control

For the outer control loop design the generalised coordinates and the mean muscle pressures are chosen as flat output candidates

$$\mathbf{y} = \mathbf{y}(\mathbf{x}, \mathbf{u}) = \begin{bmatrix} q_1 \\ q_2 \\ p_{M1} \\ p_{M2} \end{bmatrix} = \begin{bmatrix} q_1 \\ q_2 \\ \dfrac{p_{M1l} + p_{M1r}}{2} \\ \dfrac{p_{M2l} + p_{M2r}}{2} \end{bmatrix}, \qquad (26)$$

where the input vector $\mathbf{u}$ contains the four muscle pressures

$$\mathbf{u} = \begin{bmatrix} p_{M1l} & p_{M1r} & p_{M2l} & p_{M2r} \end{bmatrix}^T \qquad (27)$$

and the state vector $\mathbf{x}$ consists of the vector of generalised coordinates $\mathbf{q}$ as well as their time derivatives $\dot{\mathbf{q}}$

$$\mathbf{x} = \begin{bmatrix} \mathbf{q} \\ \dot{\mathbf{q}} \end{bmatrix}. \qquad (28)$$

The trajectory control of the mean pressure allows for increasing stiffness concerning disturbance forces acting on the end-effector (Bindel et. al., 1999). As the decentralised pressure controls have been assigned a high bandwidth, these four controlled muscle

pressures p_{Mij} can be considered as ideal control inputs of the outer control loop. Subsequent differentiation of the first two flat output candidates until one of the control appears leads to

$$
\begin{aligned}
y_1 &= q_1 \, , \\
\dot{y}_1 &= \dot{q}_1 \, , \\
\ddot{y}_1 &= \ddot{q}_1(\mathbf{q}, \dot{\mathbf{q}}, p_{M1l}, p_{M1r}),
\end{aligned}
\tag{29}
$$

and

$$
\begin{aligned}
y_2 &= q_2 \, , \\
\dot{y}_2 &= \dot{q}_2 \, , \\
\ddot{y}_2 &= \ddot{q}_2(\mathbf{q}, \dot{\mathbf{q}}, p_{M2l}, p_{M2r}) \, ,
\end{aligned}
\tag{30}
$$

whereas the third and fourth flat output candidates directly depend on the control inputs

$$
\begin{aligned}
y_3 &= p_{M1} = 0.5 \cdot (p_{M1l} + p_{M1r}), \\
y_4 &= p_{M2} = 0.5 \cdot (p_{M2l} + p_{M2r}).
\end{aligned}
\tag{31}
$$

The differential flatness can be proven as follows: all system states can be directly expressed by the flat outputs and their time derivatives

$$
\mathbf{x} = \begin{bmatrix} \mathbf{q} \\ \dot{\mathbf{q}} \end{bmatrix} = \begin{bmatrix} y_1 & y_2 & \dot{y}_1 & \dot{y}_2 \end{bmatrix}^T \, .
\tag{32}
$$

The equations of motion (9) are available in symbolic form. Inserting the muscle force characteristics, the internal muscle pressures as control inputs can be parameterized by the flat outputs and their time derivatives

$$
\mathbf{u} = \begin{bmatrix} p_{M1l}(\mathbf{q}, \dot{\mathbf{q}}, \ddot{\mathbf{q}}, p_{M1}) \\ p_{M1r}(\mathbf{q}, \dot{\mathbf{q}}, \ddot{\mathbf{q}}, p_{M1}) \\ p_{M2l}(\mathbf{q}, \dot{\mathbf{q}}, \ddot{\mathbf{q}}, p_{M2}) \\ p_{M2r}(\mathbf{q}, \dot{\mathbf{q}}, \ddot{\mathbf{q}}, p_{M2}) \end{bmatrix} = \mathbf{u}(\mathbf{q}, \dot{\mathbf{q}}, \ddot{\mathbf{q}}, p_{M1}, p_{M2}) \, .
\tag{33}
$$

In the following, three different nonlinear control approaches are employed to stabilize the error dynamics of the outer control loop: flatness-based control, backstepping and sliding-mode control (Khalil, 1996). For all these alternative designs, the differential flatness property proves advantageous (Sira-Ramirez & Llanes-Santiago, 1995; Aschemann et. al., 2007).

3.3 Flatness-based control
In the case of flatness-based control, the inverse dynamics is evaluated with the measured crank angles and the corresponding angular velocities obtained by real differentiation (Aschemann & Hofer, 2005). For the mean pressures, however, desired values are utilized. The second derivatives of the crank angles, the angular accelerations, serve as stabilizing inputs

$$
\mathbf{u} = \begin{bmatrix} p_{M1l} & p_{M1r} & p_{M2l} & p_{M2r} \end{bmatrix}^T = \mathbf{u}(\mathbf{q}, \dot{\mathbf{q}}, v_1, v_2, p_{M1d}, p_{M2d}) \, .
\tag{34}
$$

The inverse dynamics leads to a compensation of all nonlinearities. An asymptotic stabilization is achieved by pole placement with Hurwitz-polynomials for the error dynamics for each drive $i = \{1, 2\}$

$$v_i = \ddot{q}_{id} + \alpha_{i2} \cdot (\dot{q}_{id} - \dot{q}_i) + \alpha_{i1} \cdot (q_{id} - q_i) + \int_0^t \alpha_{i0} \cdot (q_{id} - q_i) d\tau \ . \tag{35}$$

3.4 Backstepping control

The first step of the backstepping control design (Khalil, 1996) involves the definition of the tracking error variable for each drive $i = \{1, 2\}$,

$$e_{i1} = q_{id} - q_i \quad \Rightarrow \quad \dot{e}_{i1} = \dot{q}_{id} - \dot{q}_i \ . \tag{36}$$

Next, a first Lyapunov function V_{i1} is introduced

$$V_{i1}(e_{i1}) = \frac{1}{2} e_{i1}^2 > 0 \quad \Rightarrow \quad \dot{V}_1(e_{i1}) = e_{i1} \cdot \dot{e}_{i1} = e_{i1} \cdot (\dot{q}_{id} - \dot{q}_i) \overset{!}{=} -c_1 \cdot e_{i1}^2 \tag{37}$$

and the expression for its time derivative is solved for the virtual control input

$$\dot{e}_{i1} = \dot{q}_{id} - \dot{q}_i = -c_1 \cdot e_{i1} \quad \Rightarrow \quad \dot{q}_i \approx \alpha_{il}(e_{i1}, \dot{q}_{id}) = \dot{q}_{id} + c_1 \cdot e_{i1} \ . \tag{38}$$

In the second step, the error variable e_{i2} is defined in the following form

$$e_{i2} = \alpha_{il}(e_{i1}, \dot{q}_{id}) - \dot{q}_i = \dot{q}_{id} - \dot{q}_i + c_1 \cdot e_{i1} \quad \Rightarrow \quad \dot{e}_{i1} = e_{i2} - c_1 \cdot e_{i1} \tag{39}$$

and its time derivative is computed

$$\dot{e}_{i2} = \ddot{q}_{id} - \ddot{q}_i + c_1 \cdot \dot{e}_{i1} = \ddot{q}_{id} - \ddot{q}_i + c_1 \cdot (e_{i2} - c_1 \cdot e_{i1}) \ . \tag{40}$$

Now, a second Lyapunov function V_{i2} is specified.

$$V_{i2}(e_{i1}, e_{i2}) = \frac{1}{2} e_{i1}^2 + \frac{1}{2} e_{i2}^2 > 0 \quad \Rightarrow \quad \dot{V}_{i2}(e_{i1}, e_{i2}) = e_{i1} \cdot \dot{e}_{i1} + e_{i2} \cdot \dot{e}_{i2} \tag{41}$$

The corresponding time derivative

$$\dot{V}_{i2}(e_{i1}, e_{i2}) = -c_1 \cdot e_{i1}^2 + e_{i2} \cdot [\ddot{q}_{id} - v_i + c_1 \cdot (e_{i2} - c_1 \cdot e_{i1}) + e_{i1}] \overset{!}{=} -c_1 \cdot e_{i1}^2 - c_2 \cdot e_{i2}^2 \tag{42}$$

can be made negative definite by choosing the stabilizing control input as follows

$$v_i = \ddot{q}_i = \ddot{q}_{id} + e_{i1} \cdot (1 - c_1^2) + e_{i2} \cdot (c_1 + c_2) \ . \tag{43}$$

Backstepping control design offers several advantages in comparison to flatness based control. It becomes possible to avoid cancellations of useful, i.e. stabilizing nonlinearities. Furthermore, different positive definite functions can be used at control design, e.g. allowing for nonlinear damping.

3.5 Sliding-mode control

For sliding-mode control (Sira-Ramirez & Llanes-Santiago, 1995) the vector of tracking errors is considered

$$\mathbf{z}_i = \begin{bmatrix} q_{id} - q_i \\ \dot{q}_{id} - \dot{q}_i \end{bmatrix} \ . \tag{44}$$

Based on this error vector $\mathbf{z}_i$, the following sliding surfaces s_i are defined for each drive $i = \{1, 2\}$

$$s_i(\mathbf{z}_i) = \dot{q}_{id} - \dot{q}_i + \beta_{i1} \cdot (q_{id} - q_i) \;\; \Rightarrow \;\; \dot{s}_i = \ddot{q}_{id} - \ddot{q}_i + \beta_{i1} \cdot (\dot{q}_{id} - \dot{q}_i), \qquad (45)$$

where β_{i1} represents a positive gain. The convergence to the corresponding sliding surface is achieved by introducing a discontinuous switching function in the time derivative of a quadratic Lyapunov function

$$V_i(s_i) = \frac{1}{2}s_i^2 \;\; \Rightarrow \;\; \dot{V}_i(s_i) = s_i \cdot \dot{s}_i \le -\alpha_i \, | \, s_i \, | = -\alpha_i \cdot s_i \cdot sign(s_i), \qquad (46)$$

with a properly chosen coefficient α_i that dominates remaining model uncertainties. The control design offers flexibility as regards the choice of the sliding surfaces and the reaching laws. For the implementation, however, a smooth switching function is preferred to reduce high frequency chattering. This results in the following stabilizing control law, which leads to a real sliding mode within a boundary layer

$$v_i = \ddot{q}_i = \ddot{q}_{id} + \beta_{i1} \cdot (\dot{q}_{id} - \dot{q}_i) + \alpha_i \cdot \tanh(\frac{s_i}{\varepsilon}). \qquad (47)$$

The implemented control structure is depicted in Fig. 8. The desired trajectories are provided from an offline trajectory planning module that calculates time optimal trajectories according to both state constraints and input constraints. This is achieved by proper time-scaling of polynomial functions with free parameters as described in (Aschemann & Hofer, 2005).
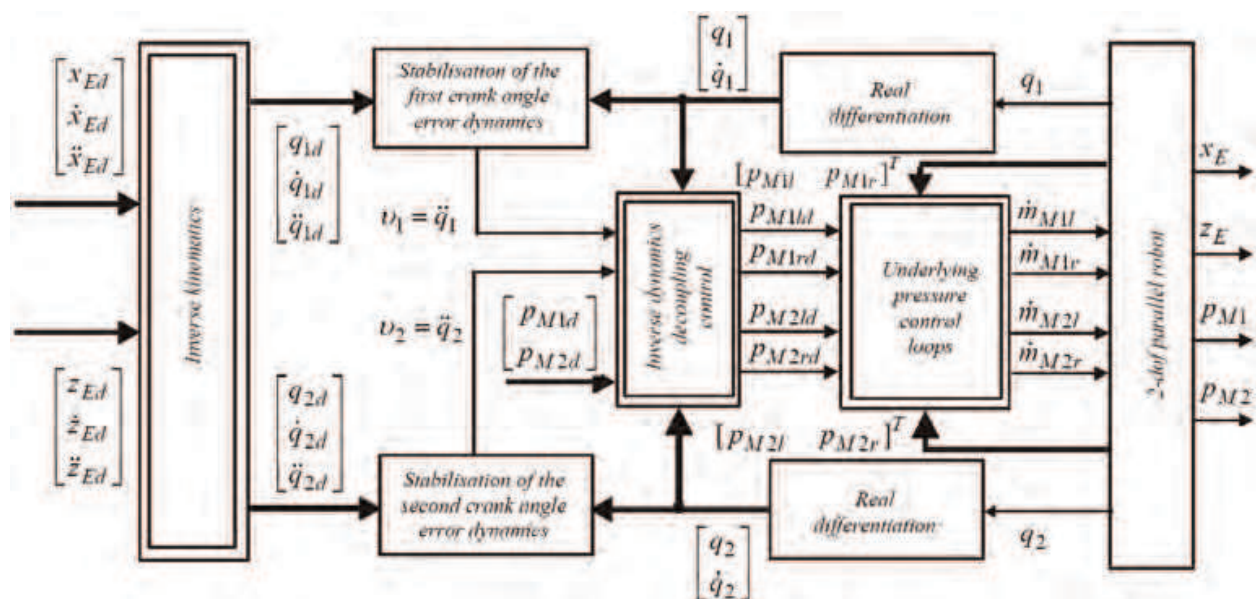

Fig. 8. Implementation of the decoupling control structure.

4. Disturbance observer design

The observer provides a vector $\hat{\mathbf{x}}_2$ of estimated disturbance torques that accounts for both model uncertainties and nonlinear friction. The main idea consists in the extension of the system state equations with the measurable state vector

$$\mathbf{y} = \mathbf{x}_1 = [\mathbf{q}, \dot{\mathbf{q}}]^T \qquad (48)$$

by two integrators, which serve as disturbance models (Aschemann et. al., 2007)

$$\begin{aligned}
\dot{\mathbf{y}} &= \mathbf{f}(\mathbf{y}, \hat{\mathbf{x}}_2, \mathbf{u}), \quad \dim(\mathbf{y}) = 4, \\
\dot{\hat{\mathbf{x}}}_2 &= \mathbf{0}, \quad \dim(\hat{\mathbf{x}}_2) = 2.
\end{aligned} \qquad (49)$$

The reduced-order disturbance observer according to (Friedland, 1996) is given by

$$\begin{aligned}
\dot{\mathbf{z}} &= \Phi(\mathbf{y}, \hat{\mathbf{x}}_2, \mathbf{u}), \quad \dim(\mathbf{z}) = 2, \\
\hat{\mathbf{x}}_2 &= \begin{bmatrix} \hat{\eta}_1 \\ \hat{\eta}_2 \end{bmatrix} = \mathbf{H}\,\mathbf{y} + \mathbf{z},
\end{aligned} \qquad (50)$$

where $\mathbf{H}$ denotes the observer gain matrix and $\mathbf{z}$ the observer state vector. The observer gain matrix is chosen as follows

$$\mathbf{H} = \begin{bmatrix} h_{11} & h_{11} & 0 & 0 \\ 0 & 0 & h_{22} & h_{22} \end{bmatrix}, \qquad (51)$$

involving only two design parameters h_{11} and h_{22}. Aiming at an asymptotically stable observer dynamics

$$\lim_{t \to \infty} \mathbf{e} = \lim_{t \to \infty}(\mathbf{x}_2 - \hat{\mathbf{x}}_2) \overset{!}{=} \mathbf{0}, \qquad (52)$$

the observer gains are determined by pole placement based on a linearization using the corresponding Jacobian (Friedland, 1996). In Fig. 9 a comparison of simulated disturbance forces and the observed forces provided by the proposed disturbance observer is shown. Here, the resulting tangential force at the pulley with radius r is depicted, which is related to the disturbance torque according to $F_{iU} = \hat{\eta}_i / r$. Obviously, the simulated disturbance forces are reconstructed with high accuracy.
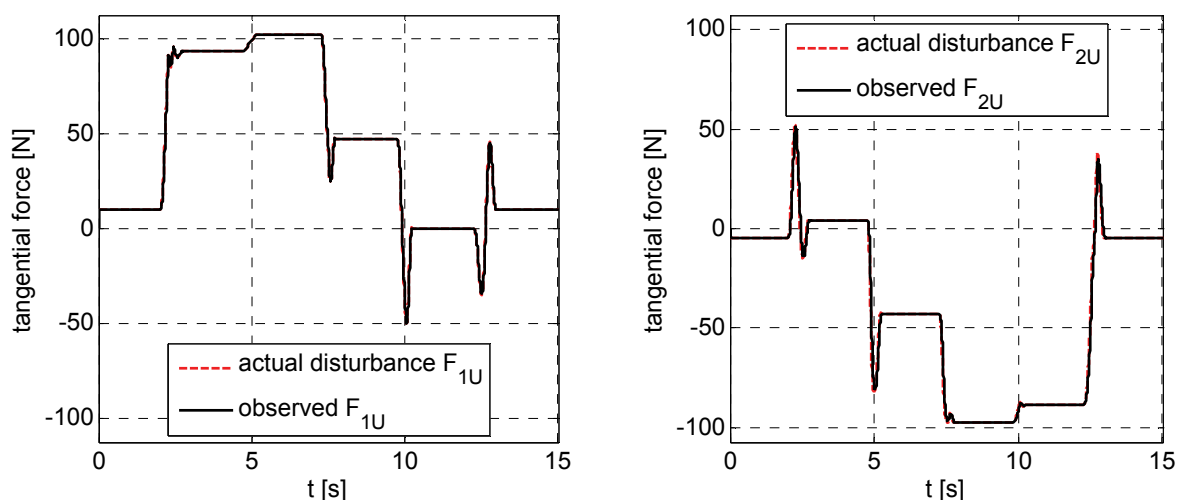

Fig. 9. Comparison of simulated disturbance force and observed disturbance force using the reduced-order disturbance observer.

5. Simulation results

The efficiency of the proposed cascade control structure is investigated using the desired trajectory shown in Fig. 10 with maximum velocities of approx. 0.9 m/s and maximum accelerations of approx. 7 m/s² for each axis.

The first part of the desired trajectory involves the motion on a quarter-circle with the radius 0.2 m from the starting point (x = 0 m, z = 1 m) to the point (x = −0.2 m, z = 0.8 m). The next three movements consist of straight lines: the second part comprises a diagonal movement in the xz-plane to the point (x = −0.1 m, z = 0.6 m), followed by a straight line motion in x-direction to the point (x = 0.1 m, z = 0.6 m). The fourth part is given by a diagonal movement to the point (x = 0.2 m, z = 0.8 m). The fifth part involves the return motion on a quarter-circle to the starting point (x = 0 m, z = 1 m).
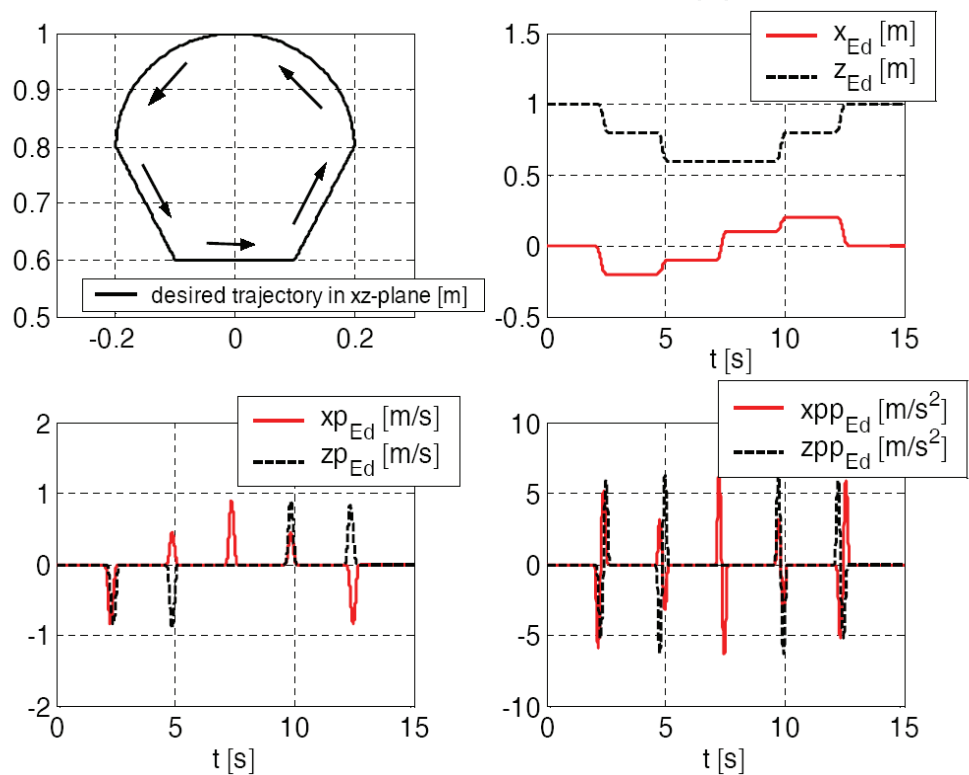
Fig. 10. Desired trajectory in the workspace.
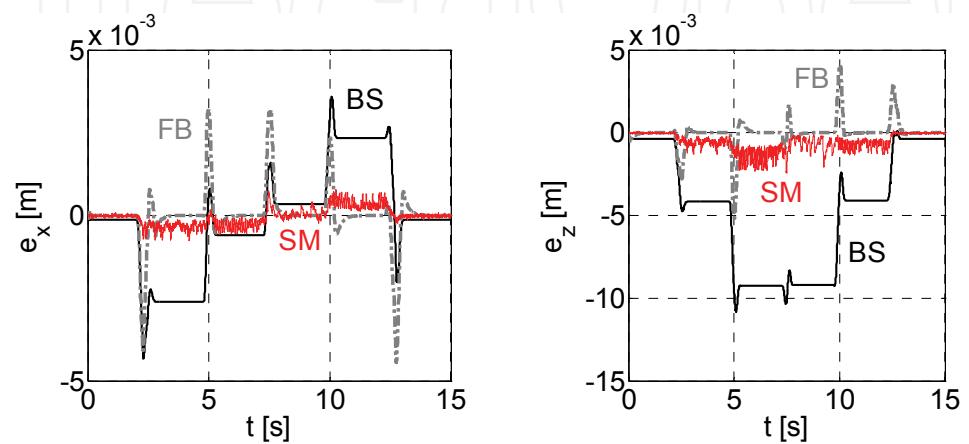
Fig. 11. Comparison of the tracking errors in the workspace without disturbance observer.

Fig. 11 shows a comparison of the resulting tracking errors in the workspace for flatness-based control (FB), backstepping control (BS) and sliding-mode control (SM). Without observer-based disturbance compensation, the best results are obtained using sliding-mode control.

The efficiency of the observer based disturbance compensation is emphasized by Fig. 12. For all considered control approaches a further improvement of tracking accuracy is achieved.

6. Conclusion

In this contribution, a cascaded trajectory control based on differential flatness is presented for a parallel robot with two degrees of freedom driven by pneumatic muscles. The modelling of this mechatronic system leads to a system of nonlinear differential equations of eighth order. For the characteristics of the pneumatic muscles polynomials serve as good approximations. The inner control loops of the cascade involve a flatness-based control of the internal muscle pressure with high bandwidth. For the outer control loop three different control approaches have been investigated leading to a decoupling of the crank angles and the mean pressures as controlled variables. Simulation results emphasize the excellent closed-loop performance with maximum position errors of approx. 1 mm during the movements, vanishing steady-state position error and steady-state pressure error of less than 0.03 bar, which have been confirmed by first experimental results at a prototype system.
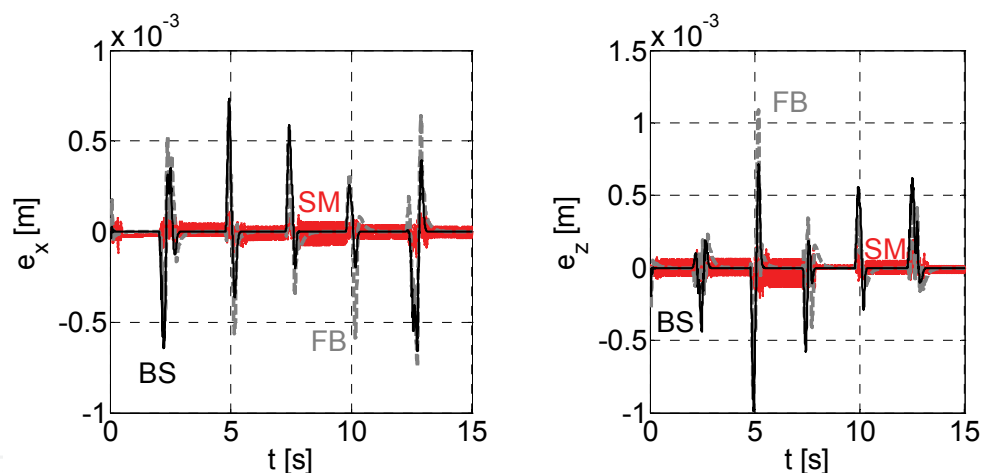

Fig. 12. Tracking errors in the workspace with observer-based disturbance compensation.

7. References

Aschemann H.; Hofer E.P. (2004). *Flatness-Based Trajectory Control of a Pneumatically Driven Carriage with Uncertainties,* CD-ROM-Proc. of NOLCOS, pp. 239 – 244, Stuttgart, September 2004

Aschemann H.; Hofer E.P. (2005). *Flatness-Based Trajectory Planning and Control of a Parallel Robot Actuated by Pneumatic Muscles,* CD-ROM-Proc. of the ECCOMAS Thematic Conference on Multibody Dynamics, Madrid, June 2005

Aschemann H.; Knestel, M.; Hofer E.P. (2007). *Nonlinear Control Strategies for a Parallel Robot Driven by Pneumatic Muscles,* Proc. of 14th Int. Workshop on Dynamics and Control, Moscow, June 2007, Nauka, Moscow

Bindel, R.; Nitsche, R.; Rothfuß, R.; Zeitz, M. (1999). *Flatness Based Control of Two Valve Hydraulic Joint Actuator of a Large Manipulator*. CD-ROM-Proc. of ECC, Karlsruhe, 1999

Carbonell P.; Jian Z.P.; Repperger D. (2001). *Comparative Study of Three Nonlinear Control Strategies for a Pneumatic Muscle Actuator*, CD-Proc. of NOLCOS, Saint-Petersburg, pp. 167 – 172, June 2001

Fliess M.; Levine J.; Martin P.; Rouchon P. (1995). *Flatness and Defect of Nonlinear Systems: Introductory Theory and Examples*, Int. J. of Control, Vol. 61, No. 6, pp. 1327 – 1361

Friedland, B. (1996). *Advanced Control System Design*, Prentice-Hall

Göttert, M. (2004). *Bahnregelung servopneumatischer Antriebe*, Berichte aus der Steuerungs- und Regelungstechnik (in German), Shaker

Khalil, H. K. (1996). *Nonlinear Systems*, 2nd. ed., Prentice-Hall

Sira-Ramirez H.; Llanes-Santiago O. (1995) *Sliding Mode Control of Nonlinear Mechanical Vibrations*, J. of Dyn. Systems, Meas. and Control, Vol. 122, No. 12, pp. 674 – 678

New Approaches in Automation and Robotics

Edited by Harald Aschemann

ISBN 978-3-902613-26-4

Hard cover, 392 pages

Publisher I-Tech Education and Publishing

Published online 01, May, 2008

Published in print edition May, 2008

The book New Approaches in Automation and Robotics offers in 22 chapters a collection of recent developments in automation, robotics as well as control theory. It is dedicated to researchers in science and industry, students, and practicing engineers, who wish to update and enhance their knowledge on modern methods and innovative applications. The authors and editor of this book wish to motivate people, especially under-graduate students, to get involved with the interesting field of robotics and mechatronics. We hope that the ideas and concepts presented in this book are useful for your own work and could contribute to problem solving in similar applications as well. It is clear, however, that the wide area of automation and robotics can only be highlighted at several spots but not completely covered by a single book.

How to reference

In order to correctly reference this scholarly work, feel free to copy and paste the following:

Harald Aschemann and Dominik Schindele (2008). Nonlinear Model-Based Control of a Parallel Robot Driven by Pneumatic Muscle Actuators, New Approaches in Automation and Robotics, Harald Aschemann (Ed.), ISBN: 978-3-902613-26-4, InTech, Available from:
http://www.intechopen.com/books/new_approaches_in_automation_and_robotics/nonlinear_model-based_control_of_a_parallel_robot_driven_by_pneumatic_muscle_actuators

INTECH
open science | open minds